Draft version December 11, 2012
Preprint typeset using LaTeX style emulateapj v. 08/22/09

arXiv:1204.4087v2 [astro-ph.EP] 8 Dec 2012

ON THE UNUSUAL GAS COMPOSITION IN THE β PICTORIS DEBRIS DISK

Ji-Wei Xie[1,2], Alexis Brandeker[3], Yanqin Wu[1]
[1]Department of Astronomy and Astrophysics, University of Toronto, Toronto, ON M5S 3H4, Canada;
jwxie@astro.utoronto.ca; wu@astro.utoronto.ca
[2]Department of Astronomy & Key Laboratory of Modern Astronomy and Astrophysics in Ministry of Education, Nanjing University, 210093, China and
[3]Department of Astronomy, Stockholm University, SE-106 91 Stockholm, Sweden; alexis@astro.su.se

Draft version December 11, 2012

ABSTRACT

The metallic gas associated with the β Pic debris disk is not believed to be primordial, but arises from the destruction of dust grains. Recent observations have shown that carbon and oxygen in this gas are exceptionally overabundant compared to other elements, by some 400 times. We study the origin of this enrichment under two opposing hypothesis, *preferential production*, where the gas is produced with the observed unusual abundance (as may happen if gas is produced by photo-desorption from C/O-rich icy grains), and *preferential depletion*, where the gas evolves to the observed state from an original solar abundance (if outgassing occurs under high-speed collisions) under a number of dynamical processes. We include in our study the following processes: radiative blow-out of metallic elements, dynamical coupling between different species, and viscous accretion onto the star. We find that, if gas viscosity is sufficiently low (the conventional α parameter $\lesssim 10^{-3}$), differential blow-out dominates. While gas accumulates gradually in the disks, metallic elements subject to strong radiation forces, such as Na and Fe, deplete more quickly than C and O, naturally leading to the observed overabundance of C and O. On the other hand, if gas viscosity is high ($\alpha \gtrsim 10^{-1}$, as expected for this largely ionized disk), gas is continuously produced and viscously accreted toward the star. This removal process does not discriminate between elements so the observed overabundance of C and O has to be explained by a *preferential production* that strongly favors C and O to other metallic elements. One such candidate is photo-desorption off the grains. We compare our calculation against all observed elements (~ 10) in the gas disk and find a mild preference for the second scenario, based on the abundance of Si alone. If true, β Pic should still be accreting at an observable rate, well after its primordial disk has disappeared.

Subject headings: circumstellar matter planetary systems: formation planetary systems: protoplanetary disks stars: individual (β Pictoris)

1. INTRODUCTION

The young (~ 20 Myr, Mentuch et al. 2008), nearby (19 pc, van Leeuwen 2007) main-sequence (A5 V) star β Pictoris has been known to harbour circumstellar (CS) gas ever since its characterization as a shell star by Slettebak (1975). With the discovery of CS dust by IRAS (Aumann 1985) located in an edge-on disk (Smith & Terrile 1984), the interest in the CS gas was renewed with more detailed observations of the circumstellar absorption lines in both the optical and the ultraviolet. The low estimated lifetime of CS dust implies that it is probably replenished on short timescales through destructive collisions, characteristic for a *debris* disk (Backman & Paresce 1993).

Early attempts to understand the properties and origin of the CS *gas* were hampered by the lack of constraints on what was believed to be the dominant gas components: H, C, N, and O. Observations of these elements are difficult because transition lines are mostly in the far-UV, where the terrestrial atmosphere blocks radiation and the stellar photospheric emission is very weak, or in the infrared (IR) to far-IR for thermal emission from molecular (H_2) or hyper-fine transitions (O I, C II), where again spectroscopic observations from space are required. Another problem was the unknown spatial distribution – absorption spectroscopy does not reveal *where* along the line of sight the gas is located, making solutions degenerate (e.g. Lagrange et al. 1995). In particular, the stellar radiation force on e.g. Na I and Ca II is known to exceed gravity by more than an order of magnitude, yet from the absorption line profile the gas is observed to be at rest with respect to the star. The problem was revisited when Olofsson et al. (2001) spatially resolved emission from Na I in orbit around the star, showing the gas to be widespread in the disk. Something must prevent the gas from escaping on free-ascend trajectories, but limits on the column density of H_2 (Lecavelier des Etangs et al. 2001) together with limits on H I (Freudling et al. 1995) shows that H cannot be dense enough in the disk to significantly brake these metal species (Brandeker et al. 2004). To solve this enigma, a variety of braking scenarios were studied by Fernández et al. (2006), who found that an overabundance of C by a factor of at least 10 over solar abundance would be sufficient for charged ions in the disk to behave as a single fluid of low effective radiation pressure and remain in orbit. C is an effective braking agent because of its high abundance, low absorption coefficient in the optical (resulting in a negligible radiation force), and an appreciable ionization fraction. Since the observed elements experiencing a high radiation force spend a tiny fraction of their time in the neutral state, it is sufficient that only ions are efficiently braked. Observations by the Far-UV Space Explorer (FUSE) subsequently showed C to indeed be overabundant by 20 × with respect to other species (Roberge et al. 2006). Recently, detailed absorption spectroscopy by HARPS at the ESO 3.6 m telescope (Brandeker 2011) and far-IR spectroscopy by Herschel/PACS of C II 157.7 μm emission from β Pic (Brandeker et al. 2012) have inferred an even higher overabundance of both C and O, up to 400 × the solar ratio.

The large amounts of C in the CS gas explains why the metallic species are not removed by the radiation pressure, but raises the new question where this huge 400 × overabundance comes from. Fernández et al. (2006) argued that the CS gas cannot be primordial, that is, a remnant from the initial star-forming nebula. Instead, the gas is thought to be secondary, and is produced by the dust grains in the debris disk, either through evaporation during mutual collisions (hereafter the ECG scenario, Czechowski & Mann 2007), or through photodesorption by UV radiation (hereafter the PDG scenario, Chen et al. 2007).[1] The two proposals produce gas with different chemical patterns: the former should lead to gas with solar-composition (hydrogen poor), the latter to C/O rich gas.

If the observed abundances reflect those at production, these observations directly reveal the production mechanism, and more importantly, the chemical composition of the dust grains. The latter property is currently unconstrained: we do not yet know whether the grains are mostly icy or rocky, or if they are depleted in carbon like bodies in our Asteroid belt. In the β Pic gas disk, not just C and O, but elements like Na, Mg, Al, Si, S, Ca, Cr, Mn, Fe, Ni are also observed. This affords us an unprecedented peek into the chemistry of planet formation in outer planetary systems.

However, the current abundances of elements in the gas might not directly reflect those at production, as the abundances could have evolved in time. In particular, the various degrees of radiation force experienced by different species may result in some elements being removed at higher rates than others. Since the radiation force on both C and O is negligible, while it is significant on most other observed elements, this could potentially explain why C and O appear enriched with respect to other elements. In this paper, we investigate the differential depletion of various elements in the β Pic disk, in an effort to explain the enrichment of C and O and to constrain the chemical composition of the dust grains. In detail, our paper is organized as follows. We describe our model in §2 with some of the detailed derivations delegated to Appendices A and B. The results are presented in §2.4. We discuss in §3 the implications of these results in the broad framework of planet formation and summarize our work in §4.

2. MODEL

We study the evolution of CS gas using a simple one-zone model. We consider elements from Li to Ni with the exceptions of noble gases. This gas is most likely second-generation gas, reproduced from solid materials after the primordial disk has dispersed. As such, the element hydrogen should be very underabundant, together with helium and other noble gases that do not easily condense. We include only the neutral and first ionized states of the elements. Higher ionization states are negligible in the β Pic disk because ionizations are mostly caused by the stellar photospheric spectrum, which has few very hard photons (Fernández et al. 2006; Zagorovsky et al. 2010). The element C, being abundant and significantly ionized, and experiencing little radiation pressure, is both the main donor of free electrons and the main braking agent (C II ions) for metal species that are radiatively accelerated. In contrast, the other abundant element, O, remains largely neutral and is considered inert. We consider four processes: 1) *Gas production*, which we assume to be continuous and due to an unspecified mechanism. 2) *Outward radiation drift.* Different gas species experience the radiation force to different degrees, parametrized by the radiation force coefficient β that is the ratio between the radiation and gravity force. For $\beta > 1$, radiation dominates over gravity. But because of the centrifugal force, $\beta > 0.5$ is sufficient for particles born on circular orbits to be unbound from the star. 3) *Field particle interaction.* Particles that are accelerated outward will interact with the field particles, C II, through Coulomb scattering. 4) *Viscous accretion.* Since the gas disk is significantly ionized, it is reasonable to assume that it is subject to the magnetorotational instability (Balbus & Hawley 1991; Hawley et al. 1995) which allows the gas to viscously accrete into the star. In the following, we will investigate how these four processes compete with each other to determine the evolution of elemental abundances.

We ignore the following processes: scattering between ions and neutral gas, and between ions and charged dust grains. Due to Coulomb focussing, ions like C II are several orders of magnitude more efficient as a braking agent, when compared to neutrals.[2] Dust, while considered by Fernández et al. (2006) as an effective braking agent, is much less efficient than C II when the number density of C II is as high as observed.

The mass of the star is $M_\star \sim 1.75\,\mathrm{M}_\odot$ and the age of the system $t_{\rm age} \sim 20\,\mathrm{Myr}$. The radiation spectrum of β Pic is adopted from Hauschildt et al. (1999), and the radiation pressure is calculated following the procedure of Fernández et al. (2006) and Zagorovsky et al. (2010). All elements are assumed to be in photo-ionization/recombination equilibrium. According to Brandeker et al. (2004), gas (at least the element sodium) follows a spatial distribution similar to that of the dust, with most gas mass located at $r \sim 100\,\mathrm{AU}$ and extending outward to hundreds of AUs. We simplify this into a one-zone model with $r = 100\,\mathrm{AU}$, assuming a disk temperature of $T_{\rm disk} \sim 50\,\mathrm{K}$ (Zagorovsky et al. 2010) and a carbon density of $N_{\rm C} = 50\,\mathrm{cm}^{-3}$, as is appropriate for the mid-plane at 100 AU (Brandeker 2011).

2.1. *Radiative Acceleration and Collisional Braking*

A particle (ion or neutral atom) with $\beta > 0.5$ is accelerated outwards by the radiation force , accompanied by

---

[1] The evaporation of comet-like bodies falling into the star (e.g. Beust et al. 1989) has also been suggested to be responsible for producing gas very close to the star.

[2] This applies even to braking atoms, as polarizability makes the ion-neutral cross-section several times larger than that of neutral-neutral interaction (Fernández et al. 2006).

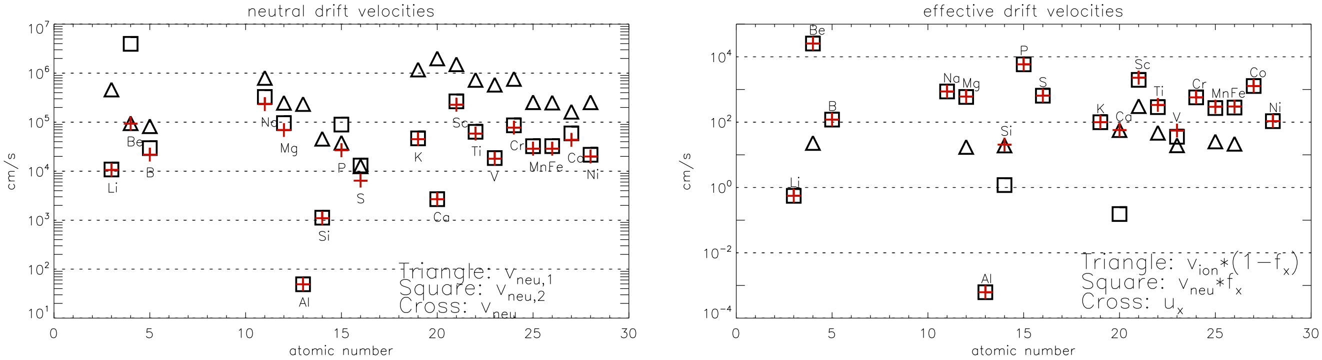

FIG. 1.— Left panel: neutral drift velocities, $v_{\rm neu,1}$ (triangles), $v_{\rm neu,2}$ (squares) and $v_{\rm neu}$ (crosses), plotted against atomic numbers for elements with $\beta > 0.5$. Most neutral species satisfy $v_{\rm neu,2} < v_{\rm neu,1}$, or, drift velocities limited by the finite ionization time. Right panel: effective drift velocities $u_{\rm x}$ (red crosses), and respective contributions from the neutral state ($f_{\rm x} v_{\rm neu}$) and from the first ionized state ($(1 - f_{\rm x}) v_{\rm ion}$), for elements that satisfy $\beta \geq 0.5$ in one or both of these states. Drift in the neutral state dominate the effective drift, with the exception of elements Si and Ca. Results are based on $N_{\rm C} = 50\,{\rm cm}^{-3}$, $r = 100\,{\rm AU}$, $T_{\rm disk} = 50\,{\rm K}$, $M_\star = 1.75\,{\rm M}_\odot$, and the radiation spectrum of a β Pic-like star.

random scattering via collisions with field particles C II. Multiplying the radiative acceleration by the mean-free-time after which the particle suffers a strong (90 deg deflection) scattering, we obtain its equilibrium outward drift velocity. Barring other processes, this velocity determines the gas removal rate from our one-zone model.

For an ion "x", this velocity is (see Appendix B)

$$v_{\rm ion} \sim 3.7\beta \left[\frac{m_{\rm x}^2}{m_{\rm C}(m_{\rm C}+m_{\rm x})}\right]^{1/2} \left(\frac{N_{\rm C\,II}}{100\,{\rm cm}^{-3}}\right)^{-1/2} \left(\frac{r}{100\,{\rm AU}}\right)^{-1} \left(\frac{M_\star}{{\rm M}_\odot}\right)^{1/2} \left(\frac{T_{\rm disk}}{100\,{\rm K}}\right)\ {\rm cm\,s}^{-1}, \quad (1)$$

where $m_{\rm C}$ and $m_{\rm x}$ are the masses of a C atom and the ion "x", respectively, r is the radial distance to the central star of mass $M_\star$, $N_{\rm C\,II}$ is the number density of C II, and $T_{\rm disk}$ is the temperature of the gas disk.

For a neutral atom "x", the equilibrium drift velocity is (see Appendix A)

$$v_{\rm neu,1} \sim 80\beta \left(\frac{m_{\rm x}}{m_{\rm C}}\right) \left(\frac{m_{\rm x} m_{\rm C}}{m_{\rm p}(m_{\rm x}+m_{\rm C})}\right)^{1/2} \left(\frac{N_{\rm C\,II}}{100\,{\rm cm}^{-3}}\right)^{-1} \left(\frac{r}{100\,{\rm AU}}\right)^{-2} \left(\frac{M_\star}{{\rm M}_\odot}\right) \left(\frac{P_{\rm x}}{10\,{\rm \AA}^3}\right)^{-1/2}\ {\rm cm\,s}^{-1}, \quad (2)$$

where $m_{\rm p}$ is the mass of the proton, and $P_{\rm x}$ the polarizability of neutral atom "x". We adopt values from Johnson (2011) (http://cccbdb.nist.gov) and where unavailable we simply take it to be $P_{\rm x} = 10^{-29}{\rm m}^{-3}$.

The typical ionization time is short for neutrals in the β Pic disk. This warrants considering the limiting velocity an atom can be accelerated to before it becomes ionized:

$$v_{\rm neu,2} \sim \beta \frac{GM_\star}{r^2}\frac{1}{\Gamma} \sim 1000\beta \left(\frac{\Gamma_{\rm x,AU}}{10^{-7}\,{\rm s}^{-1}}\right)\ {\rm cm\,s}^{-1}, \quad (3)$$

where G is the gravity constant, $\Gamma_{\rm x,AU}$ is the ionization rate of the neutral atom "x" at $r = 1\,{\rm AU}$. Following Brandeker (2011)[3], we adopt the following to be the actual drift velocity of the atom,

$$v_{\rm neu} = \frac{\gamma\, v_{\rm neu,2}}{\gamma + 1}, \quad (4)$$

where $\gamma = v_{\rm neu,1}/v_{\rm neu,2}$.

Since any given element switches between the neutral and the ionized state s, we combine $v_{\rm neu}$ and $v_{\rm ion}$ to obtain the effective drift velocity for element "x" as

$$u_{\rm x} = f_{\rm x} v_{\rm neu} + (1 - f_{\rm x}) v_{\rm ion}, \quad (5)$$

where $f_{\rm x}$ is the neutral fraction of element "x" that quantifies the fraction of time that is spent in the neutral state.

Fig. 1 shows the calculated $v_{\rm neu,1}, v_{\rm neu,2}, v_{\rm neu}$ and $v_{\rm ion}$ for all elements with $\beta > 0.5$. We observe that:

1. most elements' neutral drift velocities $v_{\rm neu}$ are close to $v_{\rm neu,2}$ (the ionization limit), except for Be and P, which are less rapidly ionized.
2. neutral drift ($v_{\rm neu} f_{\rm x}$) dominates the final effective outward drift for most elements, except for Si and Ca. The ion drift is almost completely suppressed by the strong coupling with C II.

2.2. *Radiative Acceleration versus Viscous Accretion*

The outward drift of radiatively accelerated metals is moderated by the inward diffusion in the viscous accretion disk. The latter arises in our partially ionized disk since the strong coupling between the magnetic field and the gas allows the onset of magnetorotational instability (Balbus & Hawley 1991). This instability leads to angular momentum transport to which one might ascribe a α-like turbulent diffusivity (Shakura & Sunyaev 1973)

$$\nu = \alpha v_{\rm s} h \sim \alpha \Omega_{\rm k} h^2 \quad (6)$$

where $v_{\rm s}$ is the local sound speed, h the local scale height and $\Omega_{\rm K}$ the Keplerian angular frequency. We set $h = 0.033{\rm AU}({\rm r/AU})^{5/4}$ and estimate the typical timescale s for viscous accretion and radiation driven drift to be

---

[3] Note that we use a different naming convention compared to Brandeker (2011). The two neutral limiting velocities $v_{\rm neu,1}$ and $v_{\rm neu,2}$ correspond to $v_{\rm drift}$ and $v_{\rm ion}$ in Brandeker (2011), while $v_{\rm ion}$ in this paper denotes the limiting velocity of the ionized tracer particles.

$$t_{\rm vis} \sim \frac{r^2}{\nu} \sim 1.4 \times 10^5 \left(\frac{\alpha}{0.1}\right)^{-1} \left(\frac{r}{100\,{\rm AU}}\right) \,{\rm yr} \tag{7}$$

$$t_{\rm drift} \sim \frac{r}{u_{\rm x}} \sim 4.7 \times 10^5 \left(\frac{u_{\rm x}}{100\,{\rm cm\,s^{-1}}}\right)^{-1} \left(\frac{r}{100\,{\rm AU}}\right) \,{\rm yr} \tag{8}$$

Note that $t_{\rm vis}$ is the same for all elements, while $t_{\rm drift}$ is specific to element x. Equating $t_{\rm vis}$ with $t_{\rm drift}$ we find that the critical α, at which the inward flow driven by viscous accretion is comparable to the outward flow driven by the radiation force, is given by

$$\alpha_{\rm cr} \sim 0.3 \left(\frac{u_{\rm x}}{10^3\,{\rm cm\,s^{-1}}}\right). \tag{9}$$

As is shown in the right panel of Fig. 1, many elements (Na included) have $u_{\rm x}\sim 10^3\,{\rm cm\,s^{-1}}$. So unless $\alpha \ll 10^{-1}$, the inward viscous diffusion can compete against the outward radiative drift which differentially depletes element x.

2.3. *Evolution of the Abundances*

The key quantity out of this study is the abundance ratio. We define an abundance ratio between carbon and element x as one that is normalized to the solar value (Anders & Grevesse 1989), $[{\rm C/x}] = \log_{10}(N_{\rm C}/N_{\rm x}) - \log_{10}(N_{\rm C}/N_{\rm x})_{\rm Solar}$. The observed value is $N_{\rm C}/N_{\rm Na} \approx 400(N_{\rm C}/N_{\rm Na})_{\rm Solar}$ or $[{\rm C/Na}] \approx 2.6$. It is the goal of this paper to understand how this large factor comes about.

We study a model where the gas is continuously produced at a constant rate, S_C, S_x, and with a fixed abundance ratio $[{\rm C/x}]_{\rm src}$. The value of [C/x] in the CS gas evolve in time as the element x is subject to differential removal by radiation pressure while all elements viscously diffuse to the star at the same rate. The evolution is described by the following equations

$$\begin{aligned} \frac{dN_{\rm c}}{dt} &= S_c - \frac{N_c}{t_{\rm vis}}, \\ \frac{dN_{\rm x}}{dt} &= S_x - \frac{N_x}{t_{\rm vis}} - \frac{N_x}{t_{\rm drift}}, \end{aligned} \tag{10}$$

which have solutions

$$\begin{aligned} N_{\rm c} &= S_{\rm c} t_{\rm vis}(1 - e^{-t/t_{\rm vis}}), \\ N_{\rm x} &= S_{\rm x} t_{\rm eff}(1 - e^{-t/t_{\rm eff}}), \end{aligned} \tag{11}$$

where $t_{\rm eff} = t_{\rm vis} t_{\rm drift}/(t_{\rm vis} + t_{\rm drift})$. Therefore, the evolution of the abundance ratio is

$$[{\rm C/x}] = [{\rm C/x}]_{\rm src} + \log_{10}\left[\left(\frac{t_{\rm vis}}{t_{\rm eff}}\right)\left(\frac{1 - e^{-t/t_{\rm vis}}}{1 - e^{-t/t_{\rm eff}}}\right)\right] \tag{12}$$

Elements that do not experience significant radiation pressure are easily incorporated into the above analysis by setting $t_{\rm drift} \to \infty$.

2.4. *Results*

We first focus on Na, the element with most detailed observations (Brandeker et al. 2004; Brandeker 2011; Brandeker et al. 2012).[4] Our calculations indicate that there are two possibile scenario to reproduce the observed value of $[{\rm C/Na}] \approx 2.6$. One is that the metallic gas is produced at the solar-composition, $[{\rm C/Na}]_{\rm src} \sim 0$, but experiences a negligible turbulent viscosity, $\alpha \leq 10^{-3}$. We call this *'preferential depletion'* . The other is that the gas is produced with enriched C (and O) abundances, $[{\rm C/Na}]_{\rm src} > 0$, and it is advected into the star with larger α. We call this *'preferential production'*. Our calculation places a constraint on the relationship between α and $[{\rm C/Na}]_{\rm src}$, as shown in Fig. 2. But short of other theoretical or observational evidences, both scenarios can explain the observed C/Na overabundance.

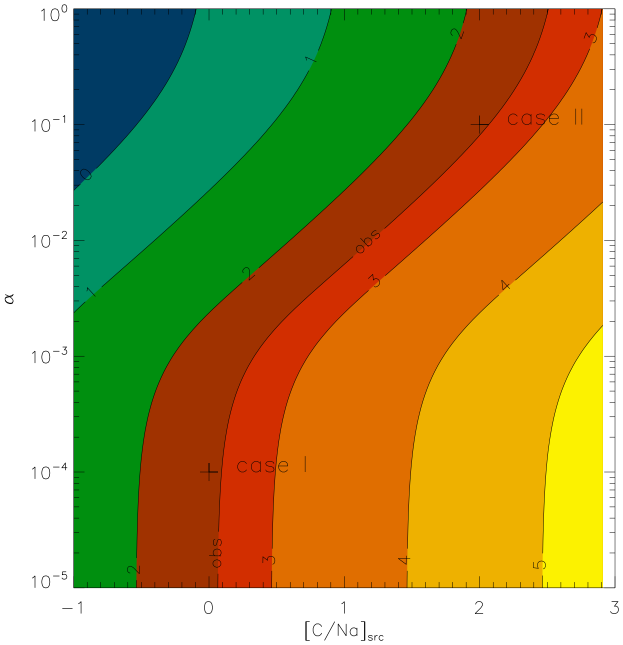

FIG. 2.— Mapping the present abundance ratio [C/Na] (normalized to the solar abundance with logarithm scale) in the $\alpha - [{\rm C/Na}]_{\rm src}$ plane. The contour line marked with "obs" denotes the abundance ratio of carbon and sodium ([C/Na] = 2.6) that is about 400 times enhanced with respect to the solar abundance, as suggested by Brandeker (2011). As expected, the present [C/Na] value increases with $[{\rm C/Na}]_{\rm src}$ and decreases for larger α. At small viscosity, e.g., $\alpha < 10^{-4}$, the viscous timescale is longer than the current age and [C/Na] becomes independent of α. In order to reproduce the observed [C/Na] value, the abundance of carbon in the gas source should be either near solar with low viscosity ($\alpha < 10^{-3}$) or super-solar with high viscosity ($\alpha > 10^{-3}$); a sub-solar abundance case can be excluded. Two crosses mark a typical solar (case I) and a typical super-solar cases (case II) that both reproduce the observed carbon enhancement. In Fig. 4, we study these cases in more detail.

Now we turn to examine other metallic species in the β Pic disk, in the hope of extracting further constraints beyond what is achieved using Na alone. We study two specific sets of parameters, both reproducing $[{\rm C/Na}] \approx 2.6$ at current time: solar abundance production and $\alpha = 10^{-4}$ (preferential depletion); and super-solar production, $[{\rm C/x}]_{\rm src} = 2$ and $\alpha = 0.1$ (preferential production). We assume for both cases that $[{\rm C/O}] = 0$, or Oxygen is produced in tandem with carbon. This is based on the considerations that O is similar to C in dynamics (experiencing only viscous diffusion), and that the observed [C/O] ≈ 0 (Brandeker et al. 2012) . The resultant [C/x] are plotted in Fig.3, and summarized in Table 1, for all elements between Li and Ni, with the exceptions of noble gases.

---

[4] While Na in the β Pic disk mostly exists in ionized form that remains invisible to us, extensive modelling efforts (Fernández et al. 2006; Zagorovsky et al. 2010) have led to estimate of the electron density (and therefore Na II/Na I ratio) that consistently reproduce the observed ionization fractions in various elements. These are listed in Table 1.

In the case of solar production (top panel of Fig. 3), the present day elemental abundances are determined by their effective drift velocities (right panel of Fig. 1), with elements that experience strong radiation drift to be severely depleted relative to C and O. This is the case for Na, Mg,P, S, Cr, Mn, Fe, Ni.[5] But we expect elements that are not radiatively accelerated, like Al, and to some degree, Si, to be undepleted relative to C and O. This expectation contrasts strongly against the observations of Si, which is detected at a value 100 times lower than our model prediction.[6] This difference is not explainable by hiding most Si in higher ionization states: in the β Pic disk, Si should be mostly in the first ionized state, which is easily observable. The observation of Al is more ambiguous. Lagrange et al. (1998) only reported a lower limit to Al since the Al II line at 1670.79 Å is very saturated. Based on the observed line profile, a rough back-of-the-envelope estimate yields that Al is likely $\sim 10^2$ more abundant than the lower limit. If true, this would place the observed Al abundance in between values expected for the two opposing scenario. The abundance of Al being crucial for deciphering the gas origin, a reanalysis of its line profile seems warranted.

The agreement between theory and observation is mildly improved in the case where the gas production is super-solar (in C and O), and where gas removal is dominated by turbulent diffusion (bottom panel of Fig. 3). The discrepancy, present still in Si, is a factor of 10 or smaller. For instance, for a production abundance of [C/x] = 3, the predicted Si is ~ 5 times higher than the observed value. In the following, we discuss the implications of these results.

3. DISCUSSION

Here, we consider other astrophysical constraints on our scenario, and what future observations may bear on our current deliberation. The implications on the process of gas generation, as well as how our results are projected in the broad picture of planet formation, are also discussed here.

3.1. *Viscosity in the gas disk*

Since the gas disk has a high ionization fraction ($\sim$ 20%), one expects it to be subject to the magnetorotational instability (MRI), which has been shown numerically to lead to turbulent viscosity of order $\alpha \sim 10^{-2}$ or higher (Hawley et al. 1995). We consider briefly the complication due to the presence of charged dust grains in the debris disk. These grains couple strongly to the charged particles (Fernández et al. 2006). The mean-free-time for electron-dust scattering is longer than the typical electron gyration time, so the electrons are expected to be tightly coupled to the magnetic field. The grains, however, may substantially enhance the resistivity. The latter effect is known to reduce α (Balbus 2009), down to values of order 10^{-4} or lower (Fleming et al. 2000; Bai & Stone 2011). A more detailed study on MRI in the presence of charged dust is required to determine the realistic α value.

3.2. *The rate of gas production and accretion*

We obtain the current total mass of the gas disk by combining the observed column densities of C in Table 1 with an assumed scale height $h \sim 0.1r$. Further assuming that C and O dominate the total gas mass and are produced at the solar ratio relative to each other, we estimate the required gas production rate to be

$$\frac{dM}{dt} \sim \begin{cases} 1.2\times10^{13}\left(\frac{\alpha}{0.1}\right)\,\mathrm{g\,s^{-1}} & \text{if } \alpha \gtrsim 7\times10^{-4} \\ 8\times10^{10}\,\mathrm{g\,s^{-1}} & \text{otherwise.} \end{cases} \qquad (13)$$

We compare these values against various models for gas production. For the solar abundance case, Czechowski & Mann (2007) estimated the gas production rate in their ECG model as $5\times10^{11}\,\mathrm{g\,s^{-1}}$ for silicate grains and $2\times10^{13}\,\mathrm{g\,s^{-1}}$ for icy grains, in the β Pic disk. These are roughly consistent with our above requirement.

Photo-desorption is a class of model where molecules and atoms are ejected from grains by UV photons. Chen et al. (2007) estimated the photo-desorption rate for Na, finding a Na production rate of $\sim 1.33\times10^{33}\,\mathrm{s^{-1}}$ for β Pic. This corresponds to a total gas production rate of $\sim 1.0\times10^{13}\,\mathrm{g\,s^{-1}}$ if photo-desorption efficiency is the same for C, N and O, as for Na. Öberg et al. (2007) performed experiments of photo-desorption of CO and CO_2 gas from icy grains. They found rates of order 10^{-3} molecules per UV photon, or, ~ 100 times higher than, e.g., those used by Chen et al. (2007) for Na. So if the dust grains have solar abundance and if all C and O are stored in the form of CO or CO_2 ice, photo-desorption would naturally yield a gas that is enriched in C and O by ~ 100 times relative to Na (and perhaps other elements). Moreover, the gas production rate would be $\sim 10^{15}\,\mathrm{g\,s^{-1}}$. So interestingly, both classes of models have no difficulty in delivering the required amount of gas. We cannot exclude either model using this discriminant.

The dust disk is also losing grains through grinding down and radiation pressure push-out. Taking a vertical optical depth of 10^{-3} for the grains at $5\,\mu$m size (blow-out size), we arrive at a rate of $\sim 10^{14}\,\mathrm{g\,s^{-1}}$ (also see Thébault & Augereau 2007). So for high α ($\alpha \geq 0.1$), the efficiency of gas production is almost comparable to the dust removal rate. We then have the intriguing possibility that dust in the β Pic disk may not be all blown away but is partially accreted back to the star in the form of gas. This possibility was also considered by Zuckerman & Song (2012) for the bright debris disk of 49 Ceti.

In the super-solar case, we expect to see the gas being predominantly channelled into the central star. Such an accretion could potentially provide an explanation for the X-ray emission observed from β Pic: the required accretion rate to explain the X-ray emission is 6.6×10^{13} – $6.6\times10^{15}\,\mathrm{g\,s^{-1}}$ (Hempel et al. 2005), compatible with the above production rates for high α's. This gas, moreover, should be highly enriched in C and O and relatively

---

[5] The CS gas of β Pic is likely of secondary origin, so a lower than solar abundance in H is not surprising.

[6] This conclusion is not significantly altered when varying α.

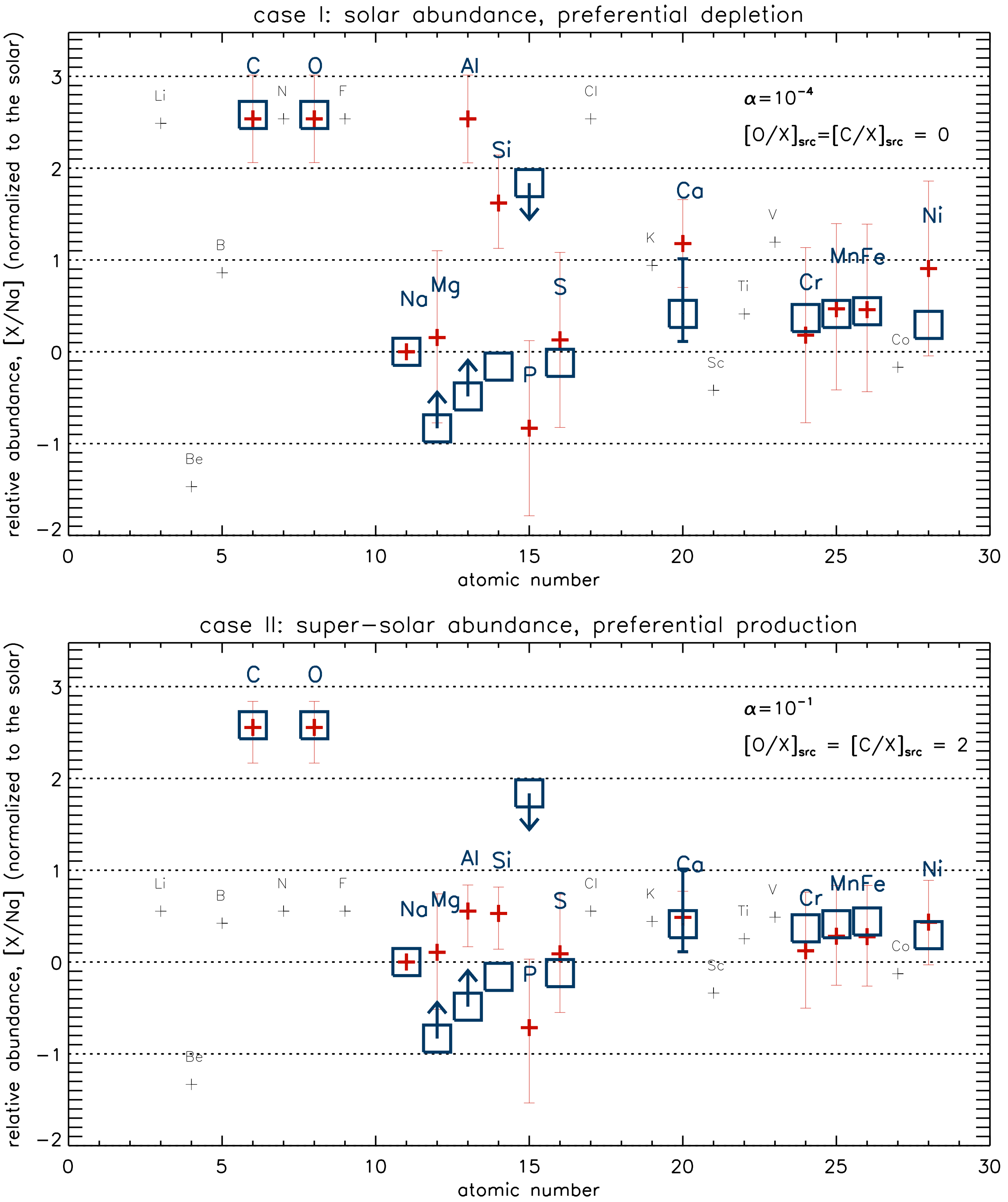
case I: solar abundance, preferential depletion

case II: super−solar abundance, preferential production

FIG. 3.— Abundance pattern in the β Pic disk, normalized to the solar value, and with all elements scaled by the element Na. The blue boxes, arrows, and errorbars represent the observed values and the red crosses the results of our calculations with the vertical red errorbars indicating effects of one source of theoretical uncertainties, when we vary the ionization fraction by a factor of 3 each way from those calculated in table 1. The top panel shows the case when all elements are produced at the solar pattern, and the viscosity is low ($\alpha = 10^{-4}$); the bottom panel shows the case when all elements are produced at the solar pattern except for C and O which are produced 100 times more abundantly, and when $\alpha = 0.1$. The size of the blue box reflects a typical uncertainty of 40% (Lagrange et al. 1998), and the arrows indicate upper limits (for P) and lower limits (for Mg and Al which have saturated absorption lines), respectively. Calculated values for elements that are as yet undetected are plotted as small black crosses. Also see Table 1 for tabulated values, as well as references for the observational ones.

TABLE 1
Column densities and Abundunces: observation vs. theory[a]

atomic number	element	neutral column density $[\mathrm{cm}^{-2}]^b$	ion column density $[\mathrm{cm}^{-2}]^b$	f_x (obs)^c	f_x (cal)^c	[x/Na] (obs)	[x/Na] (cal)^d	References
6	C	1.4×10^{17}	2.9×10^{17}	0.33	0.52	2.58	2.54; 2.55	[1]
8	O	8.6×10^{17}	-	-	~ 1	2.58	2.54; 2.55	[1]
11	Na	$(3.4 \pm 0.4) \times 10^{10}$	$[9.2 \times 10^{12}]$	-	3.7×10^{-3}	0	0; 0	[2]
12	Mg	2.5×10^{11}	$> 2.4 \times 10^{13}$	$< 1 \times 10^{-2}$	8.6×10^{-3}	> -0.83	0.15; 0.11	[3], [4]
13	Al	$< 2.7 \times 10^{12}$	$> 4.4 \times 10^{12}$	< 0.4	1.3×10^{-5}	> -0.49	2.54; 0.55	[3]
14	Si	$< 1.1 \times 10^{13}$	1.1×10^{14}	$< 1 \times 10^{-1}$	1.1×10^{-3}	-0.16	1.62; 0.53	[3]
15	P	$< 7 \times 10^{11}$	$< 9.2 \times 10^{13}$	-	0.22	< 1.8	-0.83; -0.71	[5]
16	S	5.4×10^{12}	$[4.9 \times 10^{13}]$	-	0.1	-0.12	0.13; 0.09	[3]
20	Ca	$< 2 \times 10^{9}$	$2.6^{+7.6}_{-1.2} \times 10^{13}$	$< 1.4 \times 10^{-4}$	5.7×10^{-5}	$0.41^{+0.6}_{-0.3}$	1.18; 0.49	[3],[6],[7]
24	Cr	$[3.5 \times 10^{10}]$	4.8×10^{12}	-	7.4×10^{-3}	0.37	0.18; 0.12	[3]
25	Mn	$< 2.4 \times 10^{10}$	3.8×10^{12}	$< 6 \times 10^{-3}$	9.4×10^{-3}	0.41	0.47; 0.28	[3]
26	Fe	4.9×10^{11}	1.6×10^{14}	3.1×10^{-3}	9.8×10^{-3}	0.44	0.46; 0.28	[3], [7]
28	Ni	$< 7.6 \times 10^{10}$	1.5×10^{13}	$< 5 \times 10^{-3}$	5.4×10^{-3}	0.29	0.91; 0.43	[3], [7]

References: [1] Brandeker (2011) [2] Brandeker et al. (2004), [3] Lagrange et al. (1998), [4] Vidal-Madjar et al. (1994) [5]Roberge et al. (2006), [6] Vidal-Madjar et al. (1986), [7] Crawford et al. (1994)

Note. — [a] Only elements that have reported column densities (for either neutral or first ionized state) are presented here.

Note. — [b] Observed values for column densities from absorption line studies (except C/O/Na where emission lines are detected). Most error bars are of order 40% of the measured values (Lagrange et al. 1998), unless explicitly listed. Where multiple absorption features from the same lower state are present for the same species, we adopt the largest value of column density. If the lower states are different, we add up the column densities. Values in square brackets are calculated assuming ionization equilibrium (f_x cal).

Note. — [c] Neutral fraction

Note. — [d] Abundances relative to solar, normalized by Na. Values in front of the semicolons are for the solar case, while those behind are for the super solar case (top and bottom panels of Fig. 3, respectively).

depleted in other metals. This prediction can be tested using data like those from Bouret et al. (2002).

3.3. *Carbon and Oxygen Ice-Lines*

Our result that C and O have to be produced at solar or even super-solar abundance with respect to other elements has interesting implications for the environments of proto-planetary disks. If the gas originates from grains ~ 100 AU away from β Pic, then C and O would have to be of at least solar abundance in these grains. This contrasts with both the asteroid belt bodies and the more distant cometary bodies in the solar system.

In the proto-solar nebula, the ice-line for water ice (of condensation temperature 135 K) is calculated to lie at $\sim$ 1 AU, while that for CO ice (of condensation temperature 20 K) is located at 10–100 AU, depending on disk geometry (Chiang & Goldreich 1997). The flatter the disk geometry, the closer in the ice line. Solid bodies formed between the two ice-lines would have been rich in water but carbon poor, with densities close to $1\,\mathrm{g\,cm^{-3}}$. This is indeed observed for the satellites of Jupiter and Saturn (see review by Wong et al. 2008), and for smaller Kuiper belt objects (Grundy et al. 2007; Stansberry et al. 2006).[7] Comets are also known to be significantly depleted in carbon relative to water ice, independent of whether they arrive from the Kuiper belt or the Oort cloud (Mumma & Charnley 2011). This indicates that the carbon ice-line lies outside $\sim$ 40 AU in the solar system.

Scaling from the solar model, with a stellar luminosity of $8.7L_\odot$ for β Pic, the ice-line for CO should have lied around 30–300 AU. Here, our study indicate that the carbon ice-line should have lied inward of $\sim$ 100 AU, or, the primordial disk is not very flared.

3.4. *Future Refinement*

In the present paper, we have described a local model which assumes that gas is produced at 100 AU, where most of the dust is located, and compute how the radiation force and accretion differentially act on the gas to evolve the abundances. In reality, gas is observed to extend from at least 13 AU from the central star (Brandeker et al. 2004) to hundreds of AU. If the gas is produced where most of the dust is located, the question becomes how the gas is transported inwards. One possibility is accretion triggered by MRI. To model this, however, requires a stratified model. Another assumption of our analytical model is that C II braking is efficient already from start, resulting in a constant drift velocity u_x and a constant production rate S_x for all elements "x". A more realistic scenario would be that the gas builds up over time with C II braking becoming efficient only after the C density has reached a sufficient level. A more refined model should thus take into account both the spatial extension and the evolution of the gas, to provide more precise abundance predictions for various elements, yielding stronger constraints on the origin of the gas around β Pic.

4. SUMMARY

In this paper, we investigate the unusual elemental abundance of the β Pic gas disk. We find that to attain the observed C/O rich gas using our model, the C and O gas must be produced at either solar or super-solar abundance compared to other elements; the sub-solar case is excluded. In the case of solar abundance, a low gas viscosity of $\alpha < 10^{-3}$ is required, as well as a gas production rate of $\sim 10^{11}\,\mathrm{g\,s^{-1}}$. Such a rate is achievable in the ECG model (Czechowski & Mann 2007) where gas is produced by high velocity micro-meteorites bombarding and sublimating the debris disk grains. In this scenario, the currently observed overabundance of C and O results from preferential depletion of other metallic elements by radiative acceleration.

In the case of super-solar production of C and O, a high gas viscosity is required ($\alpha \sim 0.1$), as well as a high production rate of $\sim 10^{13}\,\mathrm{g\,s^{-1}}$. Such a rate, as well as the exotic production pattern, can be satisfied by photo-desorption if the recent study on the photo-desorption of CO stands (Öberg et al. 2007). The mass in the β Pic dust disk may be partially ground down to micro meteorites that are pushed out by radiation pressure, partly outgassed and accreted into the star. The latter part may be significant. As this gas accretes into the central star, it may provide a natural explanation for the observed x-ray emission from β Pic, unusual for an A-star.

Detailed comparison between our model and the observed abundance pattern leads us to prefer the super-solar case, but only by a small margin. Our preference is informed by the fact that the column density of Si is closer to (albeit still 10 times larger than) the observed value in the super-solar case. Moreover, we argue that the gas disk should support the magnetorotational instability which yields a healthy viscosity. We propose the following tests to determine the dominant gas production mechanism:

- A re-analysis of the Al II absorption data of Lagrange et al. (1998). Since Al should not be preferentially depleted by radiation pressure, its abundance ratio relative to C and O will inform us of the production pattern.
- Analysis of UV and x-ray data like those in Bouret et al. (2002) and Hempel et al. (2005). If the x-ray does arise from gas accretion, as opposed to chromospheric activity, we can use it to determine the gas accretion rate, as well as the chemical abundances.
- The radial profile of the gas disk. If the outgassing occurs at ~ 100 AU and most of the gas accretes into the star, we expect to see gas at smaller radii. This is a particularly exciting aspect because the giant planet, β Pic b (Lagrange et al. 2010), is believed to orbit at $\sim$ 10 AU and may interact with the gas in interesting ways.

Our current model is limited in that the gas disk is approximated by a single zone at steady state. This, though unlikely to affect our basic conclusions, would need improvements to allow a more detailed comparison with observations.

---

[7] Surprisingly, large Kuiper-belt objects like Pluto and Eris are too dense ($\sim 2\,\mathrm{g\,cm^{-3}}$) to be water enriched (Null et al. 1993; Sicardy et al. 2011).

We thank the anonymous referee, as well as Philippe Thébault for the many constructive criticisms that improved the presentation of our paper. This work was initiated during the International Summer Institute for Modeling in Astrophysics (ISIMA) program held at the Kavli Institute for Astronomy and Astrophysics, Peking University. JWX was supported by the National Natural Science Foundation of China (Nos. 10833001 and 10925313), PhD training grant of China (20090091110002), and Fundamental Research Funds for the Central Universities (1112020102), and he thanks Pascale Garaud for valuable discussions and suggestions. AB was supported by the Swedish National Space Board (contract 84/08:1) and YW by the NSERC discovery grant.

REFERENCES

Anders, E., & Grevesse, N. 1989, Geochim. Cosmochim. Acta, 53, 197
Aumann, H. H. 1985, PASP, 97, 885
Backman, D. E., & Paresce, F. 1993, in Protostars and Planets III, ed. E. H. Levy & J. I. Lunine, 1253–1304
Bai, X.-N., & Stone, J. M. 2011, ApJ, 736, 144
Balbus, S. A. 2009, ArXiv e-prints
Balbus, S. A., & Hawley, J. F. 1991, ApJ, 376, 214
Beust, H., Lagrange-Henri, A. M., Vidal-Madjar, A., & Ferlet, R. 1989, A&A, 223, 304
Bouret, J.-C., Deleuil, M., Lanz, T., Roberge, A., Lecavelier des Etangs, A., & Vidal-Madjar, A. 2002, A&A, 390, 1049
Brandeker, A. 2011, ApJ, 729, 122
Brandeker, A., Liseau, R., Olofsson, G., & Fridlund, M. 2004, A&A, 413, 681
Brandeker, A., et al. 2012, subm. to A&A
Chen, C. H., et al. 2007, ApJ, 666, 466
Chiang, E. I., & Goldreich, P. 1997, ApJ, 490, 368
Crawford, I. A., Spyromilio, J., Barlow, M. J., Diego, F., & Lagrange, A. M. 1994, MNRAS, 266, L65
Czechowski, A., & Mann, I. 2007, ApJ, 660, 1541
Fernández, R., Brandeker, A., & Wu, Y. 2006, ApJ, 643, 509
Fleming, T. P., Stone, J. M., & Hawley, J. F. 2000, ApJ, 530, 464
Freudling, W., Lagrange, A.-M., Vidal-Madjar, A., Ferlet, R., & Forveille, T. 1995, A&A, 301, 231
Grundy, W. M., et al. 2007, Icarus, 191, 286
Hauschildt, P. H., Allard, F., & Baron, E. 1999, ApJ, 512, 377
Hawley, J. F., Gammie, C. F., & Balbus, S. A. 1995, ApJ, 440, 742
Hempel, M., Robrade, J., Ness, J.-U., & Schmitt, J. H. M. M. 2005, A&A, 440, 727
Johnson, R. D., ed. 2011, NIST Computational Chemistry Comparison and Benchmark Database NIST Standard Reference Database Number 101 Release 15bs
Lagrange, A. M., Vidal-Madjar, A., Deleuil, M., Emerich, C., Beust, H., & Ferlet, R. 1995, A&A, 296, 499
Lagrange, A.-M., et al. 1998, A&A, 330, 1091
—. 2010, Science, 329, 57
Lecavelier des Etangs, A., et al. 2001, Nature, 412, 706
Mentuch, E., Brandeker, A., van Kerkwijk, M. H., Jayawardhana, R., & Hauschildt, P. H. 2008, ApJ, 689, 1127
Mumma, M. J., & Charnley, S. B. 2011, ARA&A, 49, 471
Null, G. W., Owen, W. M., & Synnott, S. P. 1993, AJ, 105, 2319
Öberg, K. I., Fuchs, G. W., Awad, Z., Fraser, H. J., Schlemmer, S., van Dishoeck, E. F., & Linnartz, H. 2007, ApJ, 662, L23
Olofsson, G., Liseau, R., & Brandeker, A. 2001, ApJ, 563, L77
Roberge, A., Feldman, P. D., Weinberger, A. J., Deleuil, M., & Bouret, J.-C. 2006, Nature, 441, 724
Shakura, N. I., & Sunyaev, R. A. 1973, A&A, 24, 337
Sicardy, B., et al. 2011, Nature, 478, 493
Slettebak, A. 1975, ApJ, 197, 137
Smith, B. A., & Terrile, R. J. 1984, Science, 226, 1421
Stansberry, J. A., Grundy, W. M., Margot, J. L., Cruikshank, D. P., Emery, J. P., Rieke, G. H., & Trilling, D. E. 2006, ApJ, 643, 556
Thébault, P., & Augereau, J.-C. 2007, A&A, 472, 169
van Leeuwen, F. 2007, A&A, 474, 653
Vidal-Madjar, A., Ferlet, R., Hobbs, L. M., Gry, C., & Albert, C. E. 1986, A&A, 167, 325
Vidal-Madjar, A., et al. 1994, A&A, 290, 245
Wong, M. H., Lunine, J. I., Atreya, S. K., Johnson, T., Mahaffy, P. R., Owen, T. C., & Encrenaz, T. 2008, Reviews in Mineralogy and Geochemistry, 68, 219
Zagorovsky, K., Brandeker, A., & Wu, Y. 2010, ApJ, 720, 923
Zuckerman, B., & Song, I. 2012, ApJ, 758, 77

APPENDIX

A. EQUILIBRIUM VELOCITY DUE TO NEUTRAL-ION COLLISIONS: $V_{\mathrm{NEU},1}$

Following Beust et al. (1989), who studied the braking of ions by a neutral gas, we here consider a neutral atom braked by an ion gas (consisting of C II at a number density of $N_{\mathrm{C\,II}}$). The average net momentum loss of the neutral atom in one collision is $-m_{\mathrm{C}}\mathbf{v}$, where m_{C} is the mass of one C atom and $\mathbf{v}$ is the neutral drift velocity relative to C II, with v its magnitude. On average, the collisions are then equivalent to an effective force on the atom that can be expressed as

$$\mathbf{F}_{\mathrm{neu}} = -N_{\mathrm{C\,II}}\pi b_{\mathrm{ni}}^2 m_{\mathrm{C}} v\mathbf{v} = -k\frac{v}{v_{\mathrm{cl}}}\mathbf{v}. \tag{A1}$$

Here

$$b_{\mathrm{ni}} = \left(\frac{1}{4\pi\epsilon_0}\frac{4e^2P_{\mathrm{x}}}{\mu\, v_{\mathrm{cl}}^2}\right)^{1/4} \tag{A2}$$

is the largest impact parameter that can lead to a physical collision between the neutral and the ion, where ϵ_0 is the permittivity of free space, e is the charge of an electron, P_{x} is the polarizability of the neutral "x", $\mu = m_{\mathrm{x}}m_{\mathrm{C}}/(m_{\mathrm{x}}+m_{\mathrm{C}})$ is the reduced mass, v_{cl} is the neutral-ion collision velocity, and where

$$k = \pi m_{\mathrm{C}}\sqrt{\frac{4e^2P_{\mathrm{x}}}{4\pi\epsilon_0}\frac{N_{\mathrm{C\,II}}^2}{\mu}}. \tag{A3}$$

Two parts are contributing to the collisional velocity,

$$v_{\mathrm{cl}} \sim v_{\mathrm{s}} + v, \tag{A4}$$

where $v_{\rm s}$ is the sound speed of C II gas. The atom, on the other hand, is subject to the radiation force from the central star, which is

$$\mathbf{F}_{\rm rad} \sim \beta \frac{GM_\star m_{\rm x}}{r^2}. \tag{A5}$$

Equating $\mathbf{F}_{\rm neu}$ to $\mathbf{F}_{\rm rad}$, the equilibrium velocity can be solved as

$$v_{\rm neu,1} = \frac{F_{\rm rad} + \sqrt{F_{\rm rad}^2 + 4k\, v_{\rm s} F_{\rm rad}}}{2k}. \tag{A6}$$

This is the limiting drift velocity of a radiatively driven atom braked by neutral-ion collisions. If $v \gg v_{\rm s}$ (an assumption that here holds for most elements), then equation A4 is reduced to $v_{\rm cl} \sim v$, leading to

$$\begin{aligned} v_{\rm neu,1} &\sim F_{\rm rad}/k \qquad \text{if} \quad v \gg v_{\rm s}, \\ &= \frac{\beta}{\pi}\left(\frac{m_{\rm x}}{m_{\rm C}}\right)\left(\frac{GM_\star}{r^2}\right)\left(\frac{4e^2 P_{\rm x}}{4\pi\epsilon_0}\,\frac{N_{\rm C\,II}^2}{\mu}\right)^{-1/2}, \\ &\sim 80\beta\left(\frac{m_{\rm x}}{m_{\rm C}}\right)\left(\frac{m_{\rm x} m_{\rm C}}{m_{\rm p}(m_{\rm x}+m_{\rm C})}\right)^{1/2}\left(\frac{N_{\rm C\,II}}{100\,{\rm cm}^{-3}}\right)^{-1}\left(\frac{r}{100\,{\rm AU}}\right)^{-2}\left(\frac{M_\star}{{\rm M}_\odot}\right)\left(\frac{P_{\rm x}}{10\,\text{Å}^3}\right)^{-1/2}\,{\rm cm\,s^{-1}}, \end{aligned} \tag{A7}$$

which is the case considered by Beust et al. (1989).

B. EQUILIBRIUM VELOCITY DUE TO ION-ION COLLISIONS: $V_{\rm ION}$

Here we study the case of a tracer ion moving in C II gas. Following Beust et al. (1989), according to the classical theory of Coulomb scattering (here referred to as "collision"), the average net momentum loss of a tracer ion colliding with a C ion is

$$\delta p = -m_{\rm C}\mathbf{v}(\cos\chi - 1), \tag{B1}$$

where χ is the deflection angle given by

$$\tan\frac{\chi}{2} = \frac{1}{4\pi\epsilon_0}\frac{e^2}{\mu}\frac{1}{b v_{\rm cl}^2}, \tag{B2}$$

where b is the impact parameter. $v_{\rm cl}$ is the ion-ion impact velocity as given by equation A4. In Beust et al. (1989), they implicitly ignore v_s and take $v_{\rm cl} \sim v$. In the case we consider here, however, the tracer ion would be efficiently braked by the C II, implying $v \ll v_{\rm s}$ and $v_{\rm cl} \sim v_{\rm s}$.

The equivalent force due to ion-ion collisions can be expressed as

$$\begin{aligned} \mathbf{F}_{ion} &= v N_{\rm C\,II}\int_0^{b_{\rm max}} (\delta p) 2\pi b\; {\rm d}b \\ &= 2N_{\rm C\,II}\pi b_{\rm ii}^2 \ln\left(\frac{\mu^2}{m_{\rm C}^2}\frac{\lambda_{\rm D}^2}{b_{\rm ii}^2} + 1\right)\frac{m_{\rm C}^2}{\mu^2} m_{\rm C} v\,\mathbf{v}, \qquad \text{if} \quad v_{\rm cl} = v_{\rm s} \\ &\sim 4N_{\rm C\,II}\pi b_{\rm ii}^2 \ln\left(\frac{\lambda_{\rm D}}{b_{\rm ii}}\right)\left(1 + \frac{m_{\rm C}}{m_{\rm x}}\right) m_{\rm C} v\,\mathbf{v}. \end{aligned} \tag{B3}$$

Here $b_{\rm max}$ is the maximum acceptable value of the impact parameter, which can be taken as the Debye length

$$\lambda_{\rm D} \sim \sqrt{\frac{\epsilon_0 k_{\rm B} T_e}{e^2 n_e}} \sim \sqrt{\frac{\epsilon_0 k_{\rm B} T_{\rm disk}}{e^2 N_{\rm C\,II}}}, \qquad \text{if} \quad n_e \sim N_{\rm C\,II} \quad \text{and} \quad T_e \sim T_{\rm disk}, \tag{B4}$$

where $k_{\rm B}$ is the Boltzmann constant, T_e and $T_{\rm disk}$ are the temperatures of the electrons and the disk, respectively, and n_e is the number density of electrons. If we assume C to be the major donator of electrons, then we expect $n_e \sim N_{\rm C\,II}$. $b_{\rm ii}$ is a characteristic impact parameter for the field ion-ion collision (obtained by solving equation B2 for $\chi = 90^\circ$ and substituting μ with $m_{\rm C}$):

$$b_{\rm ii} = \frac{1}{4\pi\epsilon_0}\frac{e^2}{m_{\rm C}}\frac{1}{v_s^2} \sim \frac{1}{4\pi\epsilon_0}\frac{e^2}{k_{\rm B} T_{\rm disk}}, \tag{B5}$$

thus

$$\frac{\lambda_{\rm D}}{b_{\rm ii}} = 4\pi\,\epsilon^{3/2}\,e^{-3}\,k_{\rm B}^{3/2}\,T_{\rm disk}^{3/2}\,N_{\rm C\,II}^{-1/2}. \tag{B6}$$

Equating $\mathbf{F}_{ion}$ with $\mathbf{F}_{rad}$, we find the equilibrium velocity to be

$$\begin{aligned} v_{\rm ion} &= \left[\left(\frac{\beta}{4\ln(\lambda_{\rm D}/b_{\rm ii})}\right)\left(\frac{1}{\pi b_{\rm ii}^2 r N_{\rm C\,II}}\right)\left(\frac{m_{\rm x}^2}{m_{\rm C}(m_{\rm C}+m_{\rm x})}\right)\right]^{1/2}\left(\frac{GM_\star}{r}\right)^{1/2} \\ &\sim 3.7\beta\left[\frac{m_{\rm x}^2}{m_{\rm C}(m_{\rm C}+m_{\rm x})}\right]^{1/2}\left(\frac{N_{\rm C\,II}}{100\,{\rm cm^{-3}}}\right)^{-1/2}\left(\frac{r}{100\,{\rm AU}}\right)^{-1}\left(\frac{M_\star}{{\rm M_\odot}}\right)^{1/2}\left(\frac{T_{\rm disk}}{100\,{\rm K}}\right)\ {\rm cm\,s^{-1}}. \end{aligned} \tag{B7}$$